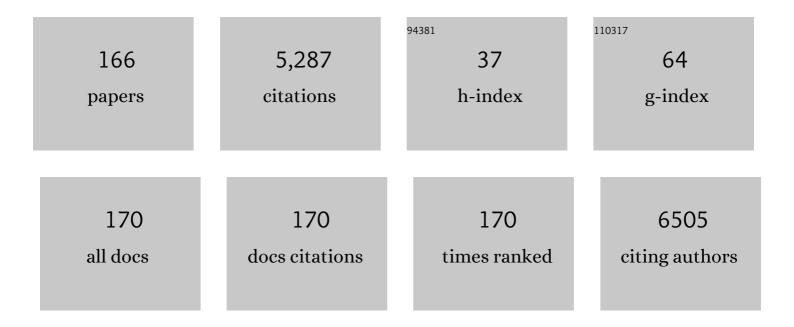
List of Publications by Year in descending order

Source: https://exaly.com/author-pdf/3398906/publications.pdf Version: 2024-02-01



RONG HUANG

#	Article	IF	CITATIONS
1	Single-atom Cu anchored catalysts for photocatalytic renewable H2 production with a quantum efficiency of 56%. Nature Communications, 2022, 13, 58.	5.8	175
2	Presence of Delocalized Ti 3d Electrons in Ultrathin Single-Crystal SrTiO <sub>3</sub> . Nano Letters, 2022, 22, 1580-1586.	4.5	2
3	Electric-Field-Induced Room-Temperature Antiferroelectric–Ferroelectric Phase Transition in van der Waals Layered GeSe. ACS Nano, 2022, 16, 1308-1317.	7.3	30
4	Three Gorges Dam: friend or foe of riverine greenhouse gases?. National Science Review, 2022, 9, .	4.6	27
5	FIB-Assisted Fabrication of Single Tellurium Nanotube Based High Performance Photodetector. Micromachines, 2022, 13, 11.	1.4	3
6	Atomic insights into the influence of Bi doping on the optical properties of two-dimensional van der Waals layered InSe. Journal of Physics Condensed Matter, 2022, 34, 224006.	0.7	1
7	Nanoscale Mapping of Cuâ€lon Transport in van der Waals Layered CuCrP <sub>2</sub> S <sub>6</sub> . Advanced Materials Interfaces, 2022, 9, .	1.9	11
8	Atomically Intimate Solid Electrolyte/Electrode Contact Capable of Surviving Long-Term Cycling with Repeated Phase Transitions. Nano Letters, 2022, 22, 3457-3464.	4.5	5
9	Gold Fractal Growth during Its Recycling from Waste Printed Circuit Boards by Slurry Electrolysis. ACS Sustainable Chemistry and Engineering, 2022, 10, 5183-5194.	3.2	5
10	Iron Single Atoms Anchored on Carbon Matrix/g-C3N4 Hybrid Supports by Single-Atom Migration-Trapping Based on MOF Pyrolysis. Nanomaterials, 2022, 12, 1416.	1.9	6
11	Iron Single Atoms Anchored on Nitrogen-Doped Carbon Matrix/Nanotube Hybrid Supports for Excellent Oxygen Reduction Properties. Nanomaterials, 2022, 12, 1593.	1.9	2
12	Twisted oxide lateral homostructures with conjunction tunability. Nature Communications, 2022, 13, 2565.	5.8	10
13	Dissolved and emitted methane in the Poyang Lake. Science China Technological Sciences, 2021, 64, 203-212.	2.0	7
14	Extremely Fast Optical and Nonvolatile Control of Mixedâ€Phase Multiferroic BiFeO <sub>3</sub> via Instantaneous Strain Perturbation. Advanced Materials, 2021, 33, e2007264.	11.1	10
15	Porous Co <sub>3</sub> O <sub>4</sub> stabilized VS <sub>2</sub> nanosheets obtained with a MOF template for the efficient HER. CrystEngComm, 2021, 23, 5097-5105.	1.3	8
16	Atomic Insights into Ti Doping on the Stability Enhancement of Truncated Octahedron LiMn2O4 Nanoparticles. Nanomaterials, 2021, 11, 508.	1.9	18
17	Multiferroic Materials: Extremely Fast Optical and Nonvolatile Control of Mixedâ€Phase Multiferroic BiFeO <sub>3</sub> via Instantaneous Strain Perturbation (Adv. Mater. 5/2021). Advanced Materials, 2021, 33, 2170035.	11.1	1
18	Revealing a high-density three-dimensional Ruddlesden–Popper-type fault network in an SmNiO3 thin film. Journal of Materials Research, 2021, 36, 1637-1645.	1.2	7

#	Article	IF	CITATIONS
19	An Environmentally Benign Cascade Reaction of 1,1-Enediamines (EDAMs) for Site-Selective Synthesis of Highly Functionalized 2,10-Dihydro-1 <i>H</i> -imidazo[1′,2′:1,6]pyrido[2,3- <i>b</i> ]indoles and Pyrroles. Journal of Organic Chemistry, 2021, 86, 5744-5756.	1.7	8
20	Cu <sub>3</sub> BiS <sub>3</sub> /MXenes with Excellent Solar–Thermal Conversion for Continuous and Efficient Seawater Desalination. ACS Applied Materials & Interfaces, 2021, 13, 16246-16258.	4.0	60
21	In-situ plasmonic tracking oxygen evolution reveals multistage oxygen diffusion and accumulating inhibition. Nature Communications, 2021, 12, 2164.	5.8	9
22	NiS <sub>2</sub> Nanocubes Coated Ti <sub>3</sub> C <sub>2</sub> Nanosheets with Enhanced Lightâ€ŧoâ€Heat Conversion for Fast and Efficient Solar Seawater Steam Generation. Solar Rrl, 2021, 5, 2100183.	3.1	13
23	Size effect of Au nanoparticles in Au-TiO2-x photocatalyst. Chemical Physics Letters, 2021, 770, 138457.	1.2	20
24	Remote growth of oxide heteroepitaxy through MoS2. APL Materials, 2021, 9, .	2.2	11
25	Electronic metal–support interaction modulates single-atom platinum catalysis for hydrogen evolution reaction. Nature Communications, 2021, 12, 3021.	5.8	397
26	Specific cation stoichiometry control of SrMnO3-Î′ thin films via RHEED oscillations. Applied Physics Letters, 2021, 118, .	1.5	2
27	Realizing N-type SnTe Thermoelectrics with Competitive Performance through Suppressing Sn Vacancies. Journal of the American Chemical Society, 2021, 143, 8538-8542.	6.6	51
28	Atomic insights into surface orientations and oxygen vacancies in the LiMn2O4 cathode for lithium storage. Journal of Alloys and Compounds, 2021, 870, 159387.	2.8	26
29	Antiferroelectric Anisotropy of Epitaxial PbHfO <sub>3</sub> Films for Flexible Energy Storage. Advanced Functional Materials, 2021, 31, 2105060.	7.8	29
30	Spin-state reconfiguration induced by alternating magnetic field for efficient oxygen evolution reaction. Nature Communications, 2021, 12, 4827.	5.8	147
31	The cell-impermeable Ru(II) polypyridyl complex as a potent intracellular photosensitizer under visible light irradiation via ion-pairing with suitable lipophilic counter-anions. Free Radical Biology and Medicine, 2021, 171, 69-79.	1.3	9
32	Highly Suppressed Thermal Conductivity in Diamond-like Cu <sub>2</sub> SnS <sub>3</sub> by Dense Dislocation. ACS Applied Energy Materials, 2021, 4, 8728-8733.	2.5	8
33	Crystallization and phase separation of tungsten oxide-bismuth vanadate amorphous film by annealing in air. Journal of Physics: Conference Series, 2021, 2011, 012102.	0.3	Ο
34	Understanding the Effect of Al Doping on the Electrochemical Performance Improvement of the LiMn <sub>2</sub> O <sub>4</sub> Cathode Material. ACS Applied Materials & Interfaces, 2021, 13, 45446-45454.	4.0	42
35	Multi-component cascade reaction of 3-formylchromones: highly selective synthesis of 4,5-dihydro-[4,5′-bipyrimidin]-6(1 <i>H</i> )-one derivatives. Chemical Communications, 2021, 57, 7657-7660.	2.2	21
36	Synergistic Modulation of the Separation of Photoâ€Generated Carriers via Engineering of Dual Atomic Sites for Promoting Photocatalytic Performance. Advanced Materials, 2021, 33, e2105904.	11.1	117

#	Article	IF	CITATIONS
37	Optimization of the In Situ Biasing FIB Sample Preparation for Hafnia-Based Ferroelectric Capacitor. Micromachines, 2021, 12, 1436.	1.4	1
38	Barium hexaferrite/muscovite heteroepitaxy with mechanically robust perpendicular magnetic anisotropy. Npj Flexible Electronics, 2021, 5, .	5.1	4
39	Protonâ€Mediated Phase Control in Flexible and Transparent Mott Transistors. Advanced Electronic Materials, 2020, 6, 1900742.	2.6	19
40	Multi-component solvent-free cascade reaction of 2-cyanoacetamides: regioselective synthesis of pyridin-2-ones bearing quaternary centers. Green Chemistry, 2020, 22, 256-264.	4.6	21
41	The effect of thickness on texture of Ge2Sb2Te5 phase-change films. Journal of Materials Science: Materials in Electronics, 2020, 31, 5848-5853.	1.1	3
42	Amorphous Metal–Organic Frameworkâ€Dominated Nanocomposites with Both Compositional and Structural Heterogeneity for Oxygen Evolution. Angewandte Chemie - International Edition, 2020, 59, 3630-3637.	7.2	143
43	Amorphous Metal–Organic Frameworkâ€Dominated Nanocomposites with Both Compositional and Structural Heterogeneity for Oxygen Evolution. Angewandte Chemie, 2020, 132, 3659-3666.	1.6	21
44	Coupling Effect of Au Nanoparticles with the Oxygen Vacancies of TiO <sub>2–<i>x</i></sub> for Enhanced Charge Transfer. Journal of Physical Chemistry C, 2020, 124, 23823-23831.	1.5	25
45	Ternary MOF-on-MOF heterostructures with controllable architectural and compositional complexity via multiple selective assembly. Nature Communications, 2020, 11, 4971.	5.8	138
46	Unexpected reversible and controllable nuclear uptake and efflux of the DNA "light-switching― Ru(ii)-polypyridyl complex in living cellsviaion-pairing with chlorophenolate counter-anions. Journal of Materials Chemistry B, 2020, 8, 10327-10336.	2.9	5
47	Nanometer-Thick Metastable Zinc Blende γ-MnTe Single-Crystalline Films for High-Performance Ultraviolet and Broadband Photodetectors. ACS Applied Nano Materials, 2020, 3, 12046-12054.	2.4	8
48	Metastable alloying structures in MAPbI3â^'xClx crystals. NPG Asia Materials, 2020, 12, .	3.8	12
49	Photoinduction of Cu Single Atoms Decorated on UiO-66-NH <sub>2</sub> for Enhanced Photocatalytic Reduction of CO <sub>2</sub> to Liquid Fuels. Journal of the American Chemical Society, 2020, 142, 19339-19345.	6.6	373
50	High-speed ultraviolet photodetectors based on 2D layered CuInP2S6 nanoflakes. Applied Physics Letters, 2020, 117, .	1.5	42
51	An environmentally benign cascade reaction of chromone-3-carboxaldehydes with ethyl 2-(pyridine-2-yl)acetate derivatives for highly site-selective synthesis of quinolizines and quinolizinium salts in water. Green Chemistry, 2020, 22, 6943-6953.	4.6	25
52	Genome-Wide Identification and Molecular Characterization of the Growth-Regulating Factors-Interacting Factor Gene Family in Tomato. Genes, 2020, 11, 1435.	1.0	10
53	Unconventional out-of-plane domain inversion <i>via</i> in-plane ionic migration in a van der Waals ferroelectric. Journal of Materials Chemistry C, 2020, 8, 6966-6971.	2.7	30
54	Boosting Oxygen and Peroxide Reduction Reactions on PdCu Intermetallic Cubes. ChemElectroChem, 2020, 7, 2614-2620.	1.7	7

#	Article	IF	CITATIONS
55	Ordered Largeâ€Pore MesoMOFs Based on Synergistic Effects of TriBlock Polymer and Hofmeister Ion. Angewandte Chemie - International Edition, 2020, 59, 14124-14128.	7.2	54
56	Ordered Largeâ€Pore MesoMOFs Based on Synergistic Effects of TriBlock Polymer and Hofmeister Ion. Angewandte Chemie, 2020, 132, 14228-14232.	1.6	12
57	Ferroelectric domain wall memory with embedded selector realized in LiNbO3 single crystals integrated on Si wafers. Nature Materials, 2020, 19, 1188-1194.	13.3	92
58	MoO <sub>2</sub> Sacrificial Layer for Optimizing Back Contact Interface of Cu <sub>2</sub> ZnSn(S,Se) <sub>4</sub> Solar Cells. IEEE Journal of Photovoltaics, 2020, 10, 1191-1200.	1.5	23
59	The Relationships of Microscopic Evolution to Resistivity Variation of a FIB-Deposited Platinum Interconnector. Micromachines, 2020, 11, 588.	1.4	3
60	High-stability fluorescent perovskites embedded in PbBrOH triggered by imidazole derivatives in water. Journal of Materials Chemistry C, 2020, 8, 5594-5599.	2.7	24
61	Improved Tensile Strength of Al-5Ce Alloy by Permanent Magnet Stirring. Metallurgical and Materials Transactions A: Physical Metallurgy and Materials Science, 2020, 51, 1972-1977.	1.1	22
62	A highly CMOS compatible hafnia-based ferroelectric diode. Nature Communications, 2020, 11, 1391.	5.8	128
63	Site-specific growth of MOF-on-MOF heterostructures with controllable nano-architectures: beyond the combination of MOF analogues. Chemical Science, 2020, 11, 3680-3686.	3.7	89
64	Sulfate-reducing bacteria (SRB) can enhance the uptake of silver-containing nanoparticles by a wetland plant. Environmental Science: Nano, 2020, 7, 912-925.	2.2	7
65	Rücktitelbild: Amorphous Metal–Organic Frameworkâ€Dominated Nanocomposites with Both Compositional and Structural Heterogeneity for Oxygen Evolution (Angew. Chem. 9/2020). Angewandte Chemie, 2020, 132, 3776-3776.	1.6	0
66	Microscopic Mechanism of Carbon-Dopant Manipulating Device Performance in CGeSbTe-Based Phase Change Random Access Memory. ACS Applied Materials & Interfaces, 2020, 12, 23051-23059.	4.0	24
67	Solvent Water Controls Photocatalytic Methanol Reforming. Journal of Physical Chemistry Letters, 2020, 11, 3738-3744.	2.1	11
68	Thickness dependence of transport behaviors in <mml:math xmlns:mml="http://www.w3.org/1998/Math/MathML"&gt;<mml:mrow><mml:mi>SrRu</mml:mi><mml:msub><mm mathvariant="normal"&gt;O<mml:mn>3</mml:mn></mm </mml:msub><mml:mo>/</mml:mo><mml:mi>SrTi<!--<br-->mathvariant="normal"&gt;O</mml:mi><mml:mn>3</mml:mn>/</mml:mrow></mml:math 	l:mi mrolgmi><	m <b>nti:</b> msub><
69	superlattices. Physical Review Materials, 2020, 4, . Revealing a metastable cubic phase in CoFe2O4–SrTiO3 three-dimensional network heteroepitaxial nanostructure. Journal of Applied Physics, 2020, 128, 225303.	1.1	0
70	Origin of Photocatalytic Activity in Ti <sup>4+</sup> /Ti <sup>3+</sup> Core–Shell Titanium Oxide Nanocrystals. Journal of Physical Chemistry C, 2019, 123, 20949-20959.	1.5	29
71	Ru subnanoparticles on N-doped carbon layer coated SBA-15 as efficient Catalysts for arene hydrogenation. Applied Catalysis A: General, 2019, 585, 117183.	2.2	21
72	Plan-view sample preparation of a buried nanodots array by FIB with accurate EDS positioning in thickness direction. Ultramicroscopy, 2019, 207, 112840.	0.8	2

#	Article	lF	CITATIONS
73	Oxygen loss and surface degradation during electrochemical cycling of lithium-ion battery cathode material LiMn <sub>2</sub> O <sub>4</sub> . Journal of Materials Chemistry A, 2019, 7, 8845-8854.	5.2	61
74	Atomically precise Ag nanoclusters intercalated in zirconium pyrophosphate for efficient hydrogenation of nitroaromatics. Applied Catalysis A: General, 2019, 574, 1-9.	2.2	20
75	Self-Template Synthesis of Nanoporous VO <sub>2</sub> -Based Films: Localized Surface Plasmon Resonance and Enhanced Optical Performance for Solar Glazing Application. ACS Applied Materials & Interfaces, 2019, 11, 22692-22702.	4.0	53
76	Hydrogenation Dynamics of Electrically Controlled Metal–Insulator Transition in Protonâ€Gated Transparent and Flexible WO 3 Transistors. Advanced Functional Materials, 2019, 29, 1902497.	7.8	21
77	Electrical polarization induced by atomically engineered compositional gradient in complex oxide solid solution. NPG Asia Materials, 2019, 11, .	3.8	4
78	Cascade Reaction of 1,1-Enediamines with 2-Benzylidene-1 <i>H</i> -indene-1,3(2 <i>H</i> )-diones: Selective Synthesis of Indenodihydropyridine and Indenopyridine Compounds. ACS Omega, 2019, 4, 6637-6646.	1.6	5
79	Anisotropic superconductivity induced by periodic multiferroic domain patterns. NPG Asia Materials, 2019, 11, .	3.8	4
80	Sensitive colorimetric detection of ochratoxin A by a dual-functional Au/Fe <sub>3</sub> O <sub>4</sub> nanohybrid-based aptasensor. RSC Advances, 2019, 9, 38590-38596.	1.7	12
81	Highly Selective Synthesis of 2-Amino-4,6-diarylpyridine Derivatives by the Cascade Reaction of 1,1-Enediamines with α,β-Unsaturated Ketones. Journal of Organic Chemistry, 2019, 84, 1999-2011.	1.7	14
82	Intergranular Oxynitride to Regulate Solution–Reprecipitation Process in Gas–Pressure‧intered SiC Ceramics with AlN–Y <sub>2</sub> O <sub>3</sub> Additives. Advanced Engineering Materials, 2019, 21, 1800821.	1.6	6
83	Structure dependence of ferroelectricity in high quality <mml:math xmlns:mml="http://www.w3.org/1998/Math/MathML"&gt; <mml:msub> <mml:mi>BiMnO</mml:mi> <mml:mn>3 epitaxial films. Physical Review Materials, 2019, 3, .</mml:mn></mml:msub></mml:math 	າ <b>ກາໄໝາອາ</b> > < /	mm/:msub><
84	Microstructure evolution determined by the crystalline phases competition in self-assembled WO3-BiVO4 hetero nanostructures. Journal of Applied Physics, 2018, 123, 085305.	1.1	4
85	Facets Matching of Platinum and Ferric Oxide in Highly Efficient Catalyst Design for Low-Temperature CO Oxidation. ACS Applied Materials & Interfaces, 2018, 10, 15322-15327.	4.0	12
86	Three-Component Site-Selective Synthesis of Highly Substituted 5 <i>H</i> -Chromeno-[4,3- <i>b</i> ]pyridines. Journal of Organic Chemistry, 2018, 83, 4981-4989.	1.7	36
87	Facile Route to the Synthesis of 1,3-Diazahetero-Cycle-Fused [1,2- <i>a</i> ]Quinoline Derivatives via Cascade Reactions. ACS Omega, 2018, 3, 1126-1136.	1.6	14
88	Inorganic sulfur and mercury speciation in the water level fluctuation zone of the Three Gorges Reservoir, China: The role of inorganic reduced sulfur on mercury methylation. Environmental Pollution, 2018, 237, 1112-1123.	3.7	31
89	Evolution of cation ordering and crystal defects controlled by Zn substitutions in Cu2SnS3 ceramics. AIP Advances, 2018, 8, 105322.	0.6	4
90	High Mobilities in Layered InSe Transistors with Indiumâ€Encapsulationâ€Induced Surface Charge Doping. Advanced Materials, 2018, 30, e1803690.	11.1	101

#	Article	IF	CITATIONS
91	Nonstoichiometric wollastonite bioceramic scaffolds with core-shell pore struts and adjustable mechanical and biodegradable properties. Journal of the Mechanical Behavior of Biomedical Materials, 2018, 88, 140-149.	1.5	18
92	Size-controlled synthesis of hierarchical bismuth selenide nanoflowers and their photocatalytic performance in the presence of H2O2. Journal of Nanoparticle Research, 2018, 20, 1.	0.8	10
93	Microstructure of Cu2S nanoprecipitates and its effect on electrical and thermal properties in thermoelectric Cu2Zn0.2Sn0.8S3 ceramics. AIP Advances, 2018, 8, 085105.	0.6	5
94	A New Defect Pyrochlore Oxide Sn <sub>1.06</sub> Nb <sub>2</sub> O <sub>5.59</sub> F <sub>0.97</sub> : Synthesis, Noble Metal Hybrids, and Photocatalytic Applications. Inorganic Chemistry, 2018, 57, 6641-6647.	1.9	11
95	Hierarchically Structured Thermoelectric Materials in Quaternary System Cu–Zn–Sn–S Featuring a Mosaic-type Nanostructure. ACS Applied Nano Materials, 2018, 1, 2579-2588.	2.4	13
96	Doubling the <i>ZT</i> record of TiS <sub>2</sub> -based thermoelectrics by incorporation of ionized impurity scattering. Journal of Materials Chemistry C, 2018, 6, 9345-9353.	2.7	22
97	Formation and dispersion of organometal halide perovskite nanocrystals in various solvents. Journal of Colloid and Interface Science, 2018, 529, 575-581.	5.0	12
98	Engineering Carbon Nanotube Fiber for Real-Time Quantification of Ascorbic Acid Levels in a Live Rat Model of Alzheimer's Disease. Analytical Chemistry, 2017, 89, 1831-1837.	3.2	71
99	Selective Synthesis of Highly Functionalized Bicyclic Pyridinone and 1,3â€Oxazinane Derivatives. European Journal of Organic Chemistry, 2017, 2017, 3442-3450.	1.2	5
100	The preparation, and structural and multiferroic properties of B-site ordered double-perovskite Bi <sub>2</sub> FeMnO <sub>6</sub> . Journal of Materials Chemistry C, 2017, 5, 5494-5500.	2.7	28
101	An environmentally benign double Michael addition reaction of heterocyclic ketene aminals with quinone monoketals for diastereoselective synthesis of highly functionalized morphan derivatives in water. Green Chemistry, 2017, 19, 3574-3584.	4.6	54
102	Aggregation induced red shift emission of phosphorus doped carbon dots. RSC Advances, 2017, 7, 32225-32228.	1.7	113
103	Aging-associated mitochondrial DNA mutations alter oxidative phosphorylation machinery and cause mitochondrial dysfunctions. Biochimica Et Biophysica Acta - Molecular Basis of Disease, 2017, 1863, 2266-2273.	1.8	30
104	Structure influence on the magnetic properties of La 0.7 Sr 0.3 MnO 3 /La 0.7 Ca 0.3 MnO 3 multilayer thin films fabricated by chemical solution deposition method. Ceramics International, 2017, 43, S497-S500.	2.3	2
105	Lattice dynamics and ferroelectric properties of the nitride perovskite <mml:math xmlns:mml="http://www.w3.org/1998/Math/MathML"&gt;<mml:msub><mml:mi>LaWN</mml:mi><mml:mn>3Physical Review B, 2017, 95, .</mml:mn></mml:msub></mml:math 	nl:nnn > <td>nm<b>48</b>nsub&gt;<!--</td--></td>	nm <b>48</b> nsub> </td
106	WO3 mesocrystal-assisted photoelectrochemical activity of BiVO4. NPG Asia Materials, 2017, 9, e357-e357.	3.8	52
107	Three-dimensional tetsubo-like Co(OH)2 nanorods on a macroporous electrically conductive network as an efficient electroactive framework for the hydrogen evolution reaction. Journal of Materials Chemistry A, 2017, 5, 2629-2639.	5.2	34
108	Cobalt-doping in Cu <sub>2</sub> SnS <sub>3</sub> : enhanced thermoelectric performance by synergy of phase transition and band structure modification. Journal of Materials Chemistry A, 2017, 5, 23267-23275.	5.2	78

#	Article	IF	CITATIONS
109	Electric field control of magnetism in nickel with coaxial cylinder structure at room temperature by electric double layer gating. Journal of Materials Chemistry C, 2017, 5, 10609-10614.	2.7	3
110	Synthesis and evaluation of the antitumor activity of highly functionalised pyridin-2-ones and pyrimidin-4-ones. RSC Advances, 2017, 7, 40067-40073.	1.7	12
111	Surface Energy Driven Cubic-to-Hexagonal Grain Growth of Ge2Sb2Te5 Thin Film. Scientific Reports, 2017, 7, 5915.	1.6	25
112	Highly efficient field emission from ZnO nanorods and nanographene hybrids on a macroporous electric conductive network. Journal of Materials Chemistry C, 2017, 5, 9296-9305.	2.7	13
113	Role of indium tin oxide electrode on the microstructure of self-assembled WO3-BiVO4 hetero nanostructures. Journal of Applied Physics, 2017, 122, .	1.1	6
114	Microstructure and electrical properties of 3-0 type composite of Na0.5Bi2.5Nb2O9-based bismuth-layered piezoceramics. Ceramics International, 2017, 43, 11710-11714.	2.3	2
115	Microstructure evolution with composition ratio in self-assembled WO <sub>3</sub> –BiVO <sub>4</sub> hetero nanostructures for water splitting. Journal of Materials Research, 2017, 32, 2790-2799.	1.2	12
116	A simulation study of inorganic sulfur cycling in the water level fluctuation zone of the Three Gorges Reservoir, China and the implications for mercury methylation. Chemosphere, 2017, 166, 31-40.	4.2	35
117	Annular Bright-Field Scanning Transmission Electron Microscopy: Direct and Robust Atomic-Resolution Imaging of Light Elements in Crystalline Materials. Microscopy Today, 2017, 25, 36-41.	0.2	7
118	Manganese molybdate nanoflakes on silicon microchannel plates as novel nano energetic material. Royal Society Open Science, 2017, 4, 171229.	1.1	5
119	Extraction of structural and chemical information from high angle annular dark-field image by an improved peaks finding method. Microscopy Research and Technique, 2016, 79, 820-826.	1.2	3
120	Control of the Metal–Insulator Transition at Complex Oxide Heterointerfaces through Visible Light. Advanced Materials, 2016, 28, 764-770.	11.1	13
121	Structure and electrical properties of epitaxial SrRuO3 thin films controlled by oxygen partial pressure. Journal of Applied Physics, 2016, 120, .	1.1	27
122	One-pot aqueous synthesis of gadolinium doped CdTe quantum dots with dual imaging modalities. Talanta, 2016, 155, 14-20.	2.9	21
123	Direct visualization of lithium via annular bright field scanning transmission electron microscopy: a review. Microscopy (Oxford, England), 2016, 66, 3-14.	0.7	20
124	A Metal–Insulator Transition of the Buried MnO <sub>2</sub> Monolayer in Complex Oxide Heterostructure. Advanced Materials, 2016, 28, 9142-9151.	11.1	17
125	Nitrogen-doped multilayered nanographene derived from Ni <sub>3</sub> C with efficient electron field emission. Journal of Materials Chemistry C, 2016, 4, 9251-9260.	2.7	9
126	Dielectric behaviors of Aurivillius Bi5Ti3Fe0.5Cr0.5O15 multiferroic polycrystals: Determining the intrinsic magnetoelectric responses by impedance spectroscopy. Scientific Reports, 2016, 5, 17846.	1.6	49

#	Article	IF	CITATIONS
127	Eco-friendly p-type Cu2SnS3 thermoelectric material: crystal structure and transport properties. Scientific Reports, 2016, 6, 32501.	1.6	96
128	Three-dimensional homo-nanostructured MnO <sub>2</sub> /nanographene membranes on a macroporous electrically conductive network for high performance supercapacitors. Journal of Materials Chemistry A, 2016, 4, 11317-11329.	5.2	24
129	Solvothermal synthesis of wire-like SnxSb2Te3+x with an enhanced thermoelectric performance. Dalton Transactions, 2016, 45, 7483-7491.	1.6	6
130	Large room-temperature magnetoresistance in epitaxial La0.7Ca0.25Sr0.05MnO3 thin films prepared by sol–gel method. Journal of Sol-Gel Science and Technology, 2016, 78, 576-581.	1.1	10
131	Epitaxial integration of a nanoscale BiFeO <sub>3</sub> phase boundary with silicon. Nanoscale, 2016, 8, 1322-1326.	2.8	8
132	Selective fabrication of n―and pâ€ŧype SnO films without doping. Physica Status Solidi - Rapid Research Letters, 2015, 9, 192-196.	1.2	18
133	Hybrid MnO <sub>2</sub> /C nano-composites on a macroporous electrically conductive network for supercapacitor electrodes. Journal of Materials Chemistry A, 2015, 3, 16695-16707.	5.2	41
134	A Facile Surfactant-Assisted Reflux Method for the Synthesis of Single-Crystalline Sb <sub>2</sub> Te <sub>3</sub> Nanostructures with Enhanced Thermoelectric Performance. ACS Applied Materials & Interfaces, 2015, 7, 14263-14271.	4.0	36
135	Hierarchical 3-dimensional CoMoO <sub>4</sub> nanoflakes on a macroporous electrically conductive network with superior electrochemical performance. Journal of Materials Chemistry A, 2015, 3, 13776-13785.	5.2	61
136	Uncovering the Formation and Selection of Benzylmalonyl-CoA from the Biosynthesis of Splenocin and Enterocin Reveals a Versatile Way to Introduce Amino Acids into Polyketide Carbon Scaffolds. Journal of the American Chemical Society, 2015, 137, 4183-4190.	6.6	43
137	Facile preparation of rare-earth semiconductor nanocrystals and tuning of their dimensionalities. RSC Advances, 2015, 5, 86885-86890.	1.7	4
138	Self-Assembly of Methyl Substituted Polyaniline Hollow Nanospheres in a Polyelectrolyte Solution. International Journal of Polymeric Materials and Polymeric Biomaterials, 2014, 63, 602-608.	1.8	7
139	Preparation and properties of epoxy resin composites containing hexaphenoxycyclotriphosphazene. High Performance Polymers, 2014, 26, 114-121.	0.8	29
140	Structural Distortion and Compositional Gradients Adjacent to Epitaxial LiMn <sub>2</sub> O <sub>4</sub> Thin Film Interfaces. Advanced Materials Interfaces, 2014, 1, 1400143.	1.9	29
141	Investigation of inclusion complex of Epothilone A with cyclodextrins. Carbohydrate Polymers, 2014, 102, 297-305.	5.1	43
142	Atomicâ€Scale Visualization of Polarization Pinning and Relaxation at Coherent BiFeO <sub>3</sub> /LaAlO <sub>3</sub> Interfaces. Advanced Functional Materials, 2014, 24, 793-799.	7.8	34
143	Facile synthesis of hollow hierarchical Ni/γ-Al <sub>2</sub> O <sub>3</sub> nanocomposites for methane dry reforming catalysis. RSC Advances, 2014, 4, 51184-51193.	1.7	50
144	Synthesis and optoelectrical properties of SnO2 nanospheres derived by microwave-assisted hydrothermal method. Applied Physics A: Materials Science and Processing, 2014, 116, 1959-1962.	1.1	2

#	Article	IF	CITATIONS
145	Epitaxial Growth of LiMn2O4 Thin Films by Chemical Solution Deposition for Multilayer Lithium-Ion Batteries. Journal of Physical Chemistry C, 2014, 118, 19540-19547.	1.5	25
146	Luminescent carbon nanoparticles as a donor for the FRET-based detection of oligonucleotide hybridization. RSC Advances, 2014, 4, 25201-25204.	1.7	3
147	Large Magnetoresistance in Magnetically Coupled SrRuO <sub>3</sub> –CoFe <sub>2</sub> O <sub>4</sub> Selfâ€Assembled Nanostructures. Advanced Materials, 2013, 25, 4753-4759.	11.1	24
148	Chemical constituents of Pteris multifida. Chemistry of Natural Compounds, 2013, 49, 629-631.	0.2	8
149	Three-component stereoselective synthesis of spirooxindole derivatives. Green Chemistry, 2013, 15, 453-462.	4.6	92
150	Threeâ€Component Synthesis of Indanoneâ€Fused Spirooxindole Derivatives. European Journal of Organic Chemistry, 2013, 2013, 4607-4613.	1.2	49
151	Morphology, thermal properties, and fire behavior of epoxy resin nanocomposites containing octaammonium polyhedral oligomeric silsesquioxane-modified montmorillonite. High Performance Polymers, 2013, 25, 992-999.	0.8	10
152	Porous V2O5 micro/nano-tubes: Synthesis via a CVD route, single-tube-based humidity sensor and improved Li-ion storage properties. Journal of Materials Chemistry, 2012, 22, 5013.	6.7	72
153	Bottom-up assembly to Ag nanoparticles embedded Nb-doped TiO2 nanobulks with improved n-type thermoelectric properties. Journal of Materials Chemistry, 2012, 22, 14180.	6.7	24
154	Dual-mode protein detection based on Fe3O4-Au hybrid nanoparticles. Nano Research, 2012, 5, 272-282.	5.8	50
155	Megastigmane O-glucopyranosides from Litsea glutinosa. Chemistry of Natural Compounds, 2012, 48, 346-349.	0.2	10
156	Structure and effect of sulfated fucose branches on anticoagulant activity of the fucosylated chondroitin sulfate from sea cucumber Thelenata ananas. Carbohydrate Polymers, 2012, 87, 862-868.	5.1	104
157	Inclusion complex of GA-13315 with cyclodextrins: Preparation, characterization, inclusion mode and properties. Carbohydrate Polymers, 2012, 89, 89-97.	5.1	23
158	Three-component solvent-free synthesis of highly substituted tetra-hydroimidazo[1,2-a]pyridines. RSC Advances, 2011, 1, 596.	1.7	22
159	Flavonoids from leaves and twigs of Stachyurus himalaicus VAR. himalaicus. Chemistry of Natural Compounds, 2011, 47, 112-113.	0.2	4
160	Chemical constituents of Litsea szemaois. Chemistry of Natural Compounds, 2011, 47, 122-123.	0.2	6
161	Optical properties of SiO2 and ZnO nanostructured replicas of butterfly wing scales. Nano Research, 2011, 4, 737-745.	5.8	18
162	Oxygenâ€Vacancy Ordering at Surfaces of Lithium Manganese(III,IV) Oxide Spinel Nanoparticles. Angewandte Chemie - International Edition, 2011, 50, 3053-3057.	7.2	127

#	Article	IF	CITATIONS
163	New Polyoxygenated Triterpenoids fromStachyurus himalaicus var.himalaicus. Helvetica Chimica Acta, 2006, 89, 2830-2835.	1.0	16
164	Insight into the microscopic morphology and electrochemical performance correlation mechanism upon calcination at different temperatures of a novel spherical cobalt-free 0.6Li2MnO3·0.4Li[Fe1/3Ni1/3Mn1/3]O2 cathode. Sustainable Energy and Fuels, 0, , .	2.5	4
165	Applying an auction optimization algorithm to mobile edge computing for security. IET Communications, 0, , .	1.5	Ο
166	An Environmentally Benign Multicomponent Cascade Reaction of 3-Formylchromones, 2-Naphthols, and Heterocyclic Ketal Aminals: Site-Selective Synthesis of Functionalized Morphan Derivatives. Journal of Organic Chemistry, 0, , .	1.7	1